JOURNAL OF THERMOPHYSICS AND HEAT TRANSFER
Vol. 25, No. 1, January–March 2011

Oxide-Film Effect on Infrared Radiative Properties of Grating Structures of Aluminum

J. Qiu* and L. H. Liu*,†
Harbin Institute of Technology, 150001 Harbin, People's Republic of China
and
P.-F. Hsu‡
Florida Institute of Technology, Melbourne, Florida 32901

DOI: 10.2514/1.49834

Aluminum tends to oxidize naturally, which hence changes the radiative properties of the metallic structure. The focus of this study is on the effect of oxide film on the infrared radiative properties of grating structures made of aluminum. Two kinds of grating-surface geometries (namely, square-wave grating and sawtooth grating) with alumina thin film are considered. The impact of the size of the oxide coating on the infrared radiative properties is predicted numerically by the finite difference time-domain method within an incident-wavelength range of 2 to 12 μm. The effect of the alumina film on the cavity resonance of square-wave gratings and the surface wave of sawtooth gratings is discussed. For the oxidized square-wave grating with a given film thickness, four different modes of cavity resonances are observed at different wavelengths. The resonance wavelengths will be changed as the oxide-film thickness increases. Because of the absorption characteristics of alumina, one mode of resonance is only formed in alumina films, while the others are excited in both alumina films and cavity. The energy of the resonance is mainly absorbed by alumina films when the resonance wavelength within the range of 10.2 to 12 μm, and it is transmitted and absorbed by aluminum substrate within the range of 2 to 10.2 μm. For the oxidized sawtooth grating, no cavity-resonance absorption peaks are observed; only one absorption peak exists, which is due to the surface waves absorbed by alumina films. The finding of this work may facilitate the design and applications of metallic gratings in cases in which the metal is easily oxidized.

Nomenclature

c	=	speed of light, m/s
$\mathbf{E}$	=	electric field vector, V/m
$\mathbf{H}$	=	magnetic field vector, A/m
j	=	$\sqrt{-1}$
$\mathbf{k}$	=	wave vector, 1/m
k_z	=	wave vector component in the z direction, 1/m
$\hat{n}$	=	complex refractive index
$\mathbf{S}$	=	Poynting vector, W/m^2
t	=	transmission coefficient or time, s
γ	=	damping term, rad/s
ε	=	relative (electric) permittivity or dielectric function
ε_0	=	permittivity of vacuum, 8.854×10^{-12} F/m
θ	=	angle, deg
κ	=	imaginary part of n
λ	=	wavelength, m
μ	=	relative (magnetic) permeability
μ_0	=	permeability of vacuum, $4\pi \times 10^{-7}$ H/m
ν_c	=	collision frequency or scattering rate, rad/s
χ	=	susceptibility
ω	=	angular frequency, rad/s
ω_0	=	resonance frequency, rad/s

Subscripts

i	=	imaginary part
p	=	plasmon
r	=	real part
x, y, z	=	x, y, and z axes in the Cartesian coordinate system

Superscript

*	=	complex conjugate

I. Introduction

THE unique radiative properties, such as resonance transmission or absorption, of metallic-grating structures have potentials in numerous applications in surface plasmon-assisted nanolithography [1], coherent thermal emission [2], and wavelength-selective thermophotovoltaic radiators [3]. In addition to the commonly studied factors of materials' properties and geometries [4–7], many other factors will also affect the radiative properties of subwavelength structures, such as surface oxidation and pollution [8,9]. It often happens that aluminum oxidizes naturally. Hence, it is important to understand how the oxide will affect the radiative properties of the metallic-grating structures.

The physical mechanism of the resonance transmission or absorption has been intensively investigated, due to surface plasmon polaritons [10], cavity resonance [11], and magnetic polaritons [12,13]. Wang et al. [11] conducted a numerical study on infrared radiative properties of heavily doped silicon complex gratings with geometric modifications and found that the resonance wavelength can be adjusted by varying the doping concentration and engineering the height of the ridges or the period. Wang and Zhang [12] provided a quantitative explanation of the phenomenon that resonance transmission or absorption observed in metallic deep gratings. They pointed out that the resonance frequency is independent of the incidence angle and strip width but depends strongly on the grating height and slit width. Lee et al. [13] demonstrated that coherent thermal emission can be achieved by exciting magnetic polaritons

Received 11 March 2010; revision received 24 July 2010; accepted for publication 7 September 2010.

*Ph.D. Candidate, School of Energy Science and Engineering, 92 West Dazhi Street; qiujun8326@163.com.
†Professor, School of Energy Science and Engineering, 92 West Dazhi Street; lhliu@hit.edu.cn (Corresponding Author).
‡Professor, Department of Mechanical and Aerospace Engineering, 150 West University Boulevard; phsu@fit.edu.

using a metallic grating coupled with a metal film. However, most previous studies just focused on the effect of materials properties and geometries of gratings on the resonance. The effects of surface oxidation on radiative properties of metallic-grating structure have not yet been studied comprehensively.

The objective of present work is to investigate the influences of oxide film on infrared radiative properties of metallic gratings. Two kinds of grating-surface geometries of aluminum coated with alumina thin film are introduced. The finite difference time-domain method is applied to solve the Maxwell's equations of wave scattering from the thin film surfaces and predict the impact of the size of the oxide coating on the infrared radiative properties within incident-wavelength range of 2 to 12 μm. The effect of the alumina film on the cavity resonance of square-wave gratings and the surface wave of sawtooth gratings is discussed. The finding of this work may facilitate the design and applications of metallic gratings in cases in which the metal is easily oxidized.

II. Numerical Methods and Model Development

A. Optical Constants and Numerical Algorithm

Optical properties of aluminum is described by Drude dispersion relation [14] as follows:

$$\varepsilon_{\mathrm{Al}} = 1 - \frac{\omega_p^2}{\omega(\omega + j \cdot \upsilon_c)} = \varepsilon_\infty + \chi(\omega) \tag{1}$$

where ω_p is the radian plasma frequency, υ_c is the collision frequency, ε_∞ is the high-frequency limiting value, and

$$\chi(\omega) = -\frac{\omega_p^2}{\omega(\omega + j\upsilon_c)}$$

is the frequency-domain susceptibility. When the temperature is 298 K, $\omega_p = 0.1976 \times 10^{17}$ rad/s and $\upsilon_c = 0.9804 \times 10^{14}$ rad/s for aluminum [14,15]. The optical properties of alumina [16] are plotted in Fig. 1, which can be transformed into complex permittivity $\varepsilon = \varepsilon_r + i\varepsilon_i = (n + ik)^2$, where $\varepsilon_r = n^2 - \kappa^2$ and $\varepsilon_i = 2n\kappa$.

Many metals in the wavelength of interest (say, infrared) have large negative ε_r. Special treatment for such a property in the difference equations is needed and discussed below.

By using convolution integral method, the frequency-domain relationship of the electric vector and displacement vector can be transformed into the time domain as [17]

$$\mathbf{D}(t) = \varepsilon_\infty \varepsilon_0 \mathbf{E}(t) + \varepsilon_0 \int_0^t \mathbf{E}(t - \Lambda)\chi(\Lambda)\, \mathrm{d}\Lambda \tag{2}$$

The preferred approach is to express the relationship between **D** and **E** in the time domain with a convolution integral as follows [17]:

$$\mathbf{D}^n = \varepsilon_\infty \varepsilon_0 \mathbf{E}^n + \varepsilon_0 \sum_{m=0}^{n-1} \mathbf{E}^{n-m} \int_{m\Delta t}^{(m+1)\Delta t} \chi(\Lambda)\, \mathrm{d}\Lambda \tag{3}$$

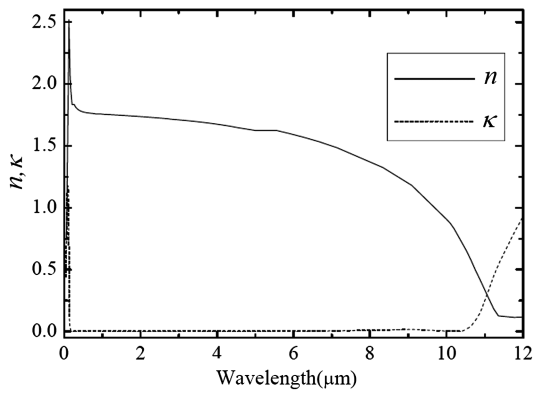

Fig. 1 Optical properties of alumina.

The value of **D** at the next time step is

$$\mathbf{D}^{n+1} = \varepsilon_\infty \varepsilon_0 \mathbf{E}^{n+1} + \varepsilon_0 \sum_{m=0}^{n} \mathbf{E}^{n+1-m} \int_{m\Delta t}^{(m+1)\Delta t} \chi(\Lambda)\, \mathrm{d}\Lambda \tag{4}$$

We now proceed to use Eqs. (3) and (4) to eliminate **D** from the dispersive finite difference time-domain equation. To simplify the algebra involved only the 1-D case is considered, but the extension to 2-D and 3-D cases is straightforward:

$$\frac{\mathbf{D}_y^{n+1}(i) - \mathbf{D}_y^n(i)}{\Delta t} = -\frac{\mathbf{H}_z^{n+\frac{1}{2}}(i + \frac{1}{2}) - \mathbf{H}_z^{n-\frac{1}{2}}(i - \frac{1}{2})}{\Delta x} - \sigma \mathbf{E}_y^{n+1}(i) \tag{5}$$

Substituting Eqs. (3) and (4) into Eq. (5) yields [17]

$$\mathbf{E}_y^{n+1}(i) = \frac{\varepsilon_\infty}{\frac{\sigma\Delta t}{\varepsilon_0} + \varepsilon_\infty + \chi^0} \mathbf{E}_y^n(i) + \frac{1}{\frac{\sigma\Delta t}{\varepsilon_0} + \varepsilon_\infty + \chi^0} \sum_{m=0}^{n-1} \mathbf{E}_y^{n-m}(i) \Delta\chi^m - \frac{\Delta t}{\frac{\sigma\Delta t}{\varepsilon_0} + \varepsilon_\infty + \chi^0} \left[\mathbf{H}_z^{n+\frac{1}{2}}\left(i + \frac{1}{2}\right) - \mathbf{H}_z^{n-\frac{1}{2}}\left(i - \frac{1}{2}\right) \right] / \varepsilon_0 \Delta x \tag{6}$$

B. Geometry

As the surface geometry of aluminum is complex, in order to facilitate analysis we only consider 1-D surface geometry structure. The computational domain is thus 2-D. The left and right edges of the computational domain boundaries are treated as periodic boundary conditions. The top and bottom sides of the computational domain are treated with Berenger's [18] perfectly-matched-layer absorbing boundary condition. Only the transverse magnetic (TM) wave incidence and normal incidence $\theta = 0°$ are considered here. For the TM wave, its magnetic field **H** oscillates perpendicularly to the plane of incidence.

The aluminum surface can easily be oxidized. The oxide film (Al_2O_3) can be generated at room temperature very quickly [19]. To simplify the analysis, the alumina layer will be reduced to a smooth film. The geometry of the periodic structure of bare aluminum surface is shown in Fig. 2, and that coated with alumina film is shown in Fig. 3 (where b, d, and c dimensions represent different thicknesses of alumina film coated on different parts of the aluminum

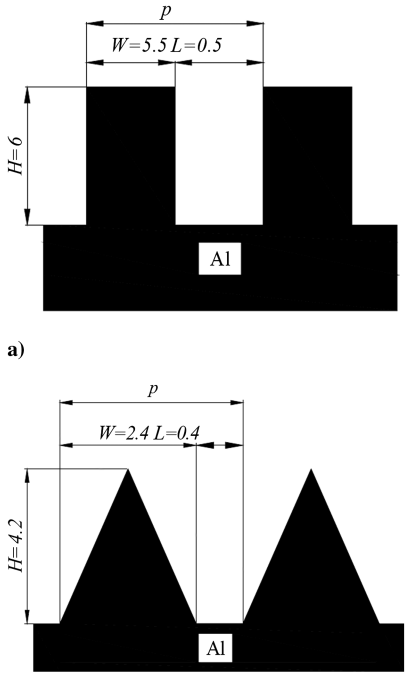

Fig. 2 Schematic of two different periodic geometries of aluminum: a) case A and b) case B; units are in microns and p is the period.

surface). The wavelength range of interest in the present study is the midinfrared band: namely, 2 to 12 μm.

Figure 2 shows the cases of two different periodic geometries of aluminum. In Fig. 2a, the geometry of a binary grating is defined by its ridge height $H = 6$ μm, ridge width $W = 5.5$ μm, and groove width $L = 0.5$ μm. Figure 2b shows the geometry of a triangular profile grating defined by its ridge height $H = 4.2$ μm, ridge width $W = 2.4$ μm, and groove width $L = 0.4$ μm. It is further assumed that the aluminum is sufficiently thick and the substrate can be modeled as semi-infinite.

The cases of two different periodic geometries of aluminum coated with alumina, namely, square-wave-shaped grating (case A) and sawtooth-shaped grating (case B), are depicted in Figs. 3a and 3b, respectively. The local coordinate is defined for each case, and values of all dimensions (including p, H, W, and L) are the same as those in Fig. 2. Radiative properties of periodic geometries of aluminum without alumina film serve as reference.

III. Results and Discussion

A. Case A: Square-Wave Gratings

The physical mechanism of the reflectance minimum from metallic gratings has been intensively investigated regarding cavity resonance [20]. The resonance wavelength is not only affected by the period of grating structures, but also by the geometries of grating, including ridge height H, ridge width W, and groove width L. This was also shown similarly in [12]. This paper mainly focuses on the oxide-film effects on the radiative properties. The spectral reflectances for TM waves of the square-wave aluminum grating coated with oxide film are illustrated in Fig. 4. It can be seen that the minimum reflectance of aluminum (solid line) is observed at $\lambda = 5.3$ and 9 μm. The spectral reflectance of alumina-coated aluminum is plotted with dashed lines. The dashed lines with symbols (triangles or rectangles) indicate different alumina-film thicknesses. It is observed that four resonance wavelengths appear when the alumina-film thickness increases. The four resonance wavelengths (RWs) are designated as RW1, RW2, RW3, and RW4 in Fig. 4. RW1 shifts toward a shorter wavelength, but the magnitude is almost the same. RW2 is almost unchanged, but the magnitude increases. RW3 and RW4 shift toward a longer wavelength and the magnitude reduces. RW2 behaves differently from RW3 and RW4, as the thickness of alumina increases, which may be caused by the effect of the oxide films of different locations. It is clear that the spectral location of the reflectance minimum is very sensitive to alumina film. The reflectances of RW1, RW2, and RW3 are less than that of the square-wave aluminum grating, while that for RW4 is almost the same. That is to say, the cavity resonance of aluminum grating can be affected by the oxide film. Further confirmation of the effect of the oxide film on cavity resonance and its corresponding electromagnetic (EM) fields will be shown in following section.

Figure 4 shows that the deep minimum observed at $\lambda = 9$ μm for the uncoated case (the black solid line) comes from the cavity resonance, which can be analyzed by the time-average Poynting vector and square of the z-component magnetic field strength, as shown in Fig. 5. The Poynting vector is defined by [21]

$$\mathbf{S} = 0.5 \cdot \mathrm{Re}[\mathbf{E} \times \mathbf{H}^*] \tag{7}$$

where Re denotes the real part of the complex quantity, and $\mathbf{E}$ and $\mathbf{H}^*$ are the electric field vector and complex conjugate of the magnetic field vector, respectively. The Poynting vector is normalized to that of incidence, whose wavelength is 9 μm.

In Fig. 5a, the time-averaged Poynting vectors around the grating region are plotted for grating case A (without Al_2O_3) at normal incidence. The grating profile is marked by white lines for easy identification. The arrows indicate the direction of the Poynting vector as well as the path of net energy flow. The magnitude of Poynting vector inside gratings is greater than that above the gratings and marked with different shades. The energy is squeezed into the narrow gratings with negligible reflectance from the grating surface. Figure 5b shows the corresponding magnetic fields in one period of grating case A. A clear cavity resonance is shown. The magnetic field strength inside gratings is higher than that above the grating structure.

The cavity-resonance mode and roles of alumina film can be further investigated by exhibiting the Poynting vector $\mathbf{S}$ and EM fields around gratings. The grating aluminum (case A) coated with alumina size $b = d = c = 0.5$ μm at normal incidence and four spectral locations of minima ($\lambda = 10.9$, 9.6, 7.3, and 6.1 μm) are taken as examples, shown in Fig. 6. Poynting vectors in Fig. 6a at $\lambda = 10.9$ μm clearly show the metal-surface plasmon and the incident-wave polarization coupling in the alumina films coated on both sides of the ridge. Poynting vectors are mostly guided into alumina films, forming standing waves. The difference with grating aluminum without alumina films, as in Fig. 5, is that the case A ($b = d = c = 0.5$ μm) structure does not form a standing wave inside the cavity. That is to say, the energy flow is attracted mainly in the form of a standing wave in the alumina films coated on both sides of the ridge. The constants of the optical properties of alumina are

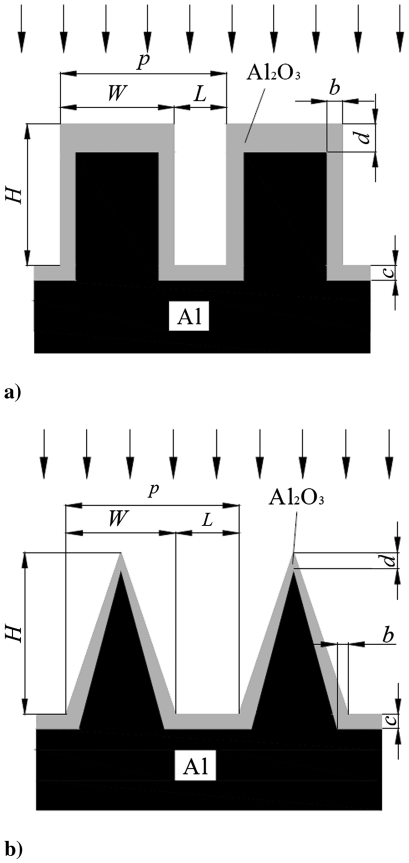

Fig. 3 Schematic of two different periodic geometries of aluminum coated with alumina, where b, d, and c are the dimensions of alumina on the different positions: a) case A and b) case B.

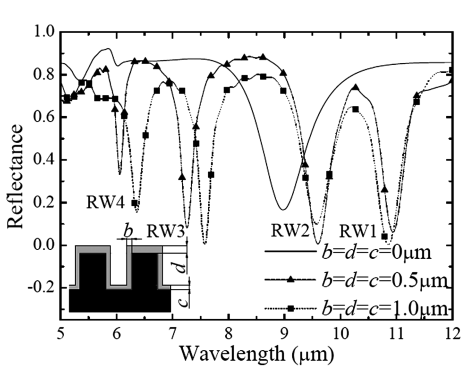

Fig. 4 Spectral reflectance of aluminum coated with alumina (case A) for TM waves at $\theta = 0°$.

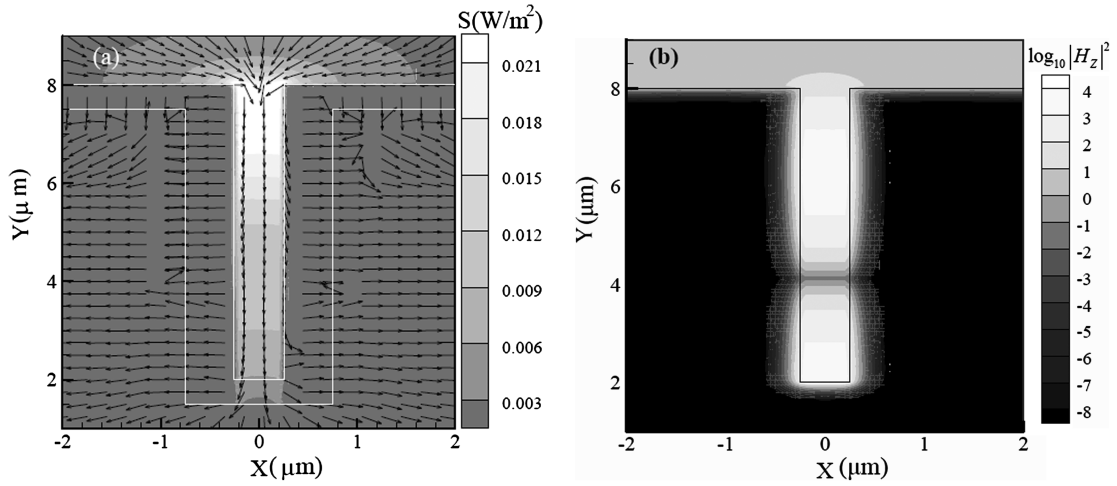

Fig. 5 Poynting vectors and the magnitude square of the complex magnetic field in the logarithmic scale for grating case A (without Al_2O_3) at $\theta = 0°$ and $\lambda = 9.0$ μm ($p/\lambda = 0.667$ with 0.170 reflectance: a) Poynting vectors and b) square of the complex magnetic field strength in the logarithmic scale.

shown in Fig. 1; at the incident wavelength of 10.9 μm, the extinction coefficient κ of alumina is about 0.4. Note that the extinction coefficient is directly related to the spectral absorption. Therefore, the energy of the standing wave is mainly absorbed by the alumina films at the incidence wavelength of 10.9 μm, which is also confirmed by Fig. 7a. Figure 7a shows the square of the complex magnetic field strength at the incident wavelength of 10.9 μm and the reflectance of 0.075. From this figure we can see the energy in the alumina films coated on both sides of ridge is almost the same as the energy in the cavity. When this is compared with Figs. 7b–7d, the energy in the alumina film and the cavity is much less than RW2, RW3, and RW4, but the reflectance of RW1 is almost the same as RW2 and RW3, as shown in Fig. 4. So the energy of the standing waves is mainly absorbed by the alumina film, which is demonstrated as mentioned before. Figure 6b shows the Poynting vectors at $\lambda = 9.6$ μm and the reflectance of 0.0058. It is clear that the metal-surface plasmon and the incident-wave polarization coupling in the alumina films are coated on both sides of the convex ridge and the

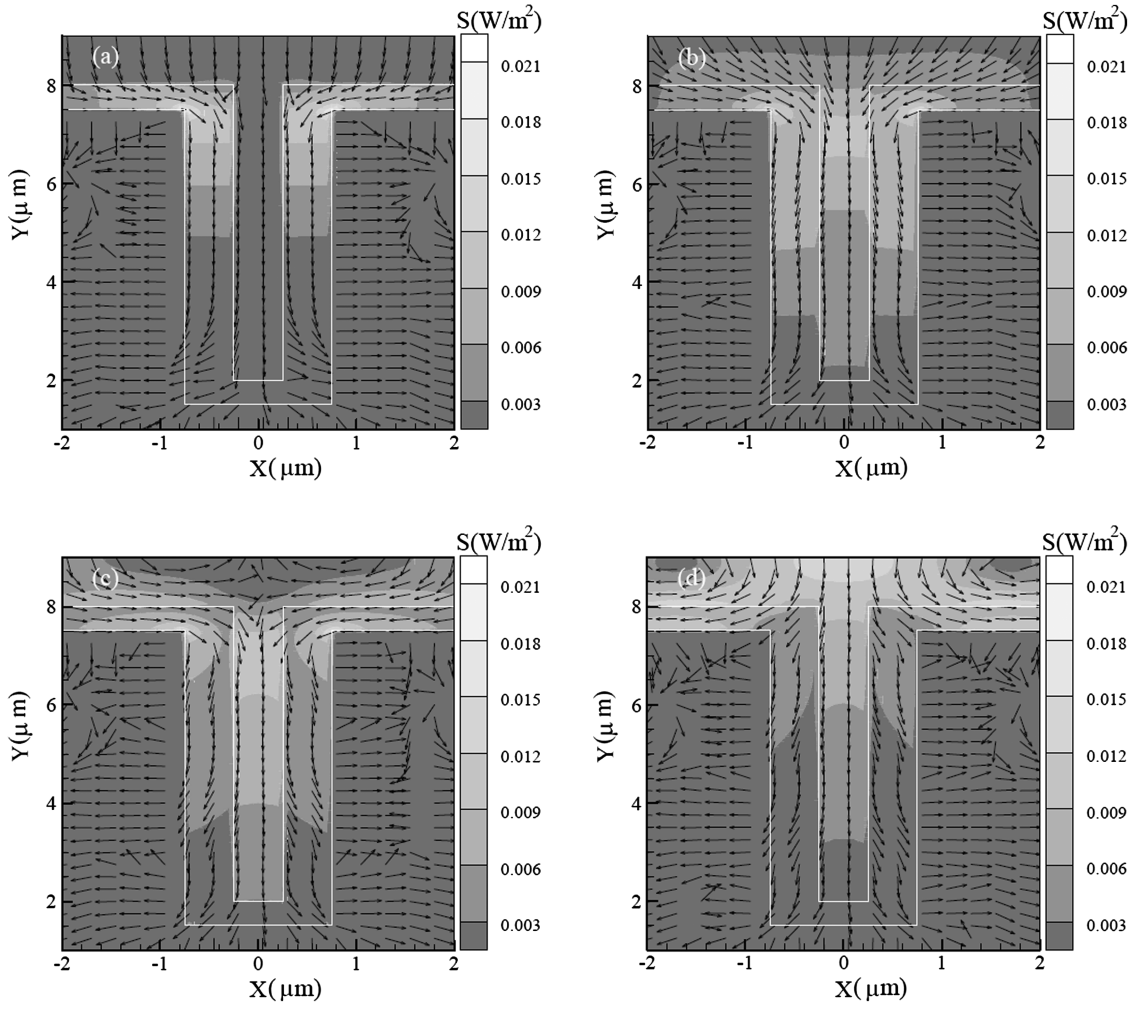

Fig. 6 Poynting vectors for grating case A ($b = d = c = 0.5$ μm) at $\theta = 0°$: a) $\lambda = 10.9$ μm, b) $\lambda = 9.6$ μm, c) $\lambda = 7.3$ μm, and d) $\lambda = 6.1$ μm.

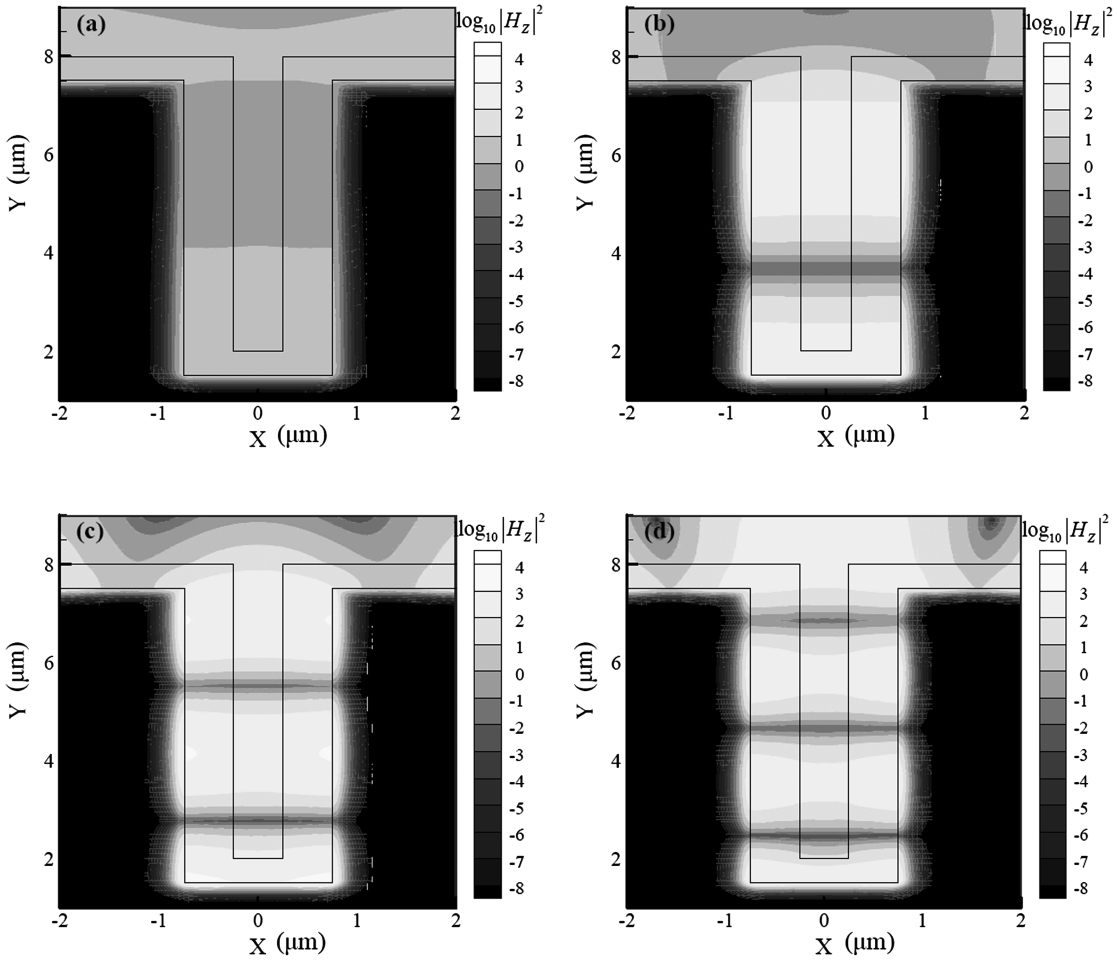

Fig. 7 Square of the complex magnetic field strength in the logarithmic scale for grating case A ($b = d = c = 0.5\ \mu$m) at $\theta = 0°$: a) $\lambda = 10.9\ \mu$m, b) $\lambda = 9.6\ \mu$m, c) $\lambda = 7.3\ \mu$m, and d) $\lambda = 6.1\ \mu$m.

cavity. Poynting vectors are mostly guided into alumina films and the cavity, forming standing waves. Referring to the optical constants of alumina shown in Fig. 1, when the wavelength increases from 2 to 10.2 μm, the n value decreases from 1.7 to 0.6, but the κ value stays at 0. Therefore, the alumina film does not absorb the energy. And the energy is absorbed by the aluminum when the incident wavelength is from 2 to 10.2 μm. This is confirmed by Fig. 7b, which shows the square of the complex magnetic field strength at the incident wavelength of 9.6 μm. From this figure we can see that the energy in the alumina films coated on both sides of convex ridge is almost the same as the energy in the cavity and much more than that in Fig. 7a. The interference forms a standing wave in the alumina films coated on both sides of ridge as well as in the cavity. The reason for the minimum at the wavelengths of RW3 and RW4 is the same as for RW2 and is not repeated here.

B. Case B: Sawtooth Gratings

The oxide-film effects on the spectral reflectance of the sawtooth aluminum grating for TM waves are illustrated in Fig. 8 by individually changing b, d, or c from parameters listed in Table 1. The deep reflectance minimum can be observed at $\lambda = 11.4\ \mu$m of coated aluminum in Fig. 8a. On the contrary, the spectral reflectance of uncoated aluminum (the solid line) does not have an obvious reflectance minimum. The figure also shows that the spectral reflectance of aluminum coated with 0.2 μm alumina is almost the same as that of 0.4 μm alumina. That is to say, the thickness of alumina films does not produce significant effect on the spectral reflectance. Figure 8b shows that the aluminum base surface, either coated or uncoated with alumina (case B), produces little effect on the spectral reflectance; specifically, the location and magnitude of the minimum do not change with the alumina thickness c.

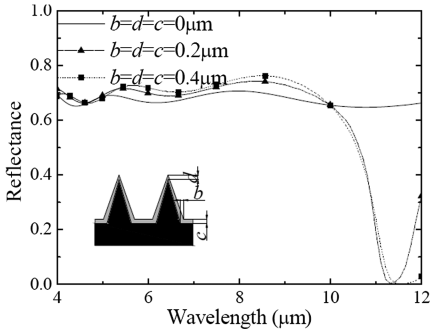

a)

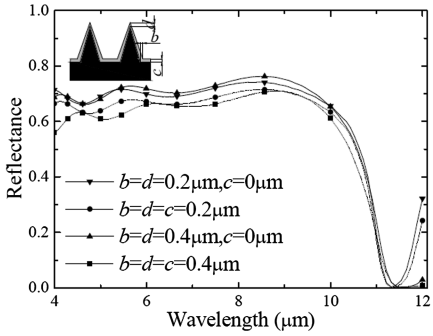

b)

Fig. 8 Spectral reflectance of aluminum coated with alumina (case B) for TM waves at $\theta = 0°$.

Table 1 Coating dimension of case B grating structures

Case B	b, μm	d, μm	c, μm
1	0	0	0
2	0.2	0.2	0.2
3	0.4	0.4	0.4
4	0.2	0.2	0
5	0.4	0.4	0

The reasons for the reflectance minimum in Fig. 8 are discussed below. Figure 9 plots Poynting vectors and the square of the complex magnetic field strength in the logarithmic scale for grating case B-1 (without Al_2O_3) at normal incidence. It is clear that the spectral reflectance of aluminum without coating does not have a deep minimum, as shown in Fig. 8a. That is to say, the sawtooth aluminum grating cannot form a cavity resonance in the wavelength range of 4 to 12 μm. In Fig. 9a, arrowheads tell the directions of Poynting vectors, such that the path of net energy flow is clear. The EM propagates toward the bottom of the cavity along the sides of the ridge. A surface wave can be observed clearly in this figure. Such a wave is associated with surface plasmon polaritons, resulting from the interaction of photons in the dielectric material and electrons in the metal. A high angle between the surface plane and incidence wave is required to excite a surface wave. This was demonstrated in [22] and is not repeated here.

Poynting vectors and the square of the complex magnetic field strength in the logarithmic scale for grating case B-2 ($b = d = c = 0.2$ μm) for TM waves at normal incidence and $\lambda = 11.4$ μm are plotted in Fig. 10. The reasons for the formation of reflectance minimum can be further investigated by comparing Figs. 9 and 10 and noting the following:

1) The deep minimum of the spectral reflectance of coated aluminum (case B-2) observed at $\lambda = 11.4$ μm is mainly due to the alumina optical properties and surface wave. The optical constant of alumina (Fig. 1) at the incident wavelength of 11.4 μm the κ value is about 0.7, so it can absorb the surface wave energy. This is the same reason that the alumina film (case A) can absorb part of the standing-wave energy at the incident wavelength of 10.9 μm.

2) Radiative properties are dependent on the grating and coating structure. When the incident wavelength is 10.9 μm, the metal-surface plasmon and the incident-wave polarization are coupled in the alumina films coated on both sides of the ridge (case A). Poynting vectors are mostly guided into alumina films and forming standing waves. However, no standing wave is formed inside the cavity. The energy flow is attracted mainly in the form of standing waves in the alumina films coated on both sides of ridge, whereas the surface waves are forming in the alumina film of the case B-2 structure. The energy of the surface wave is mainly absorbed by the alumina film on both sides of the ridge, as shown in Fig. 10b. In other words, the magnitude of the reflectance minimum depends on the structure and optical constants of alumina film.

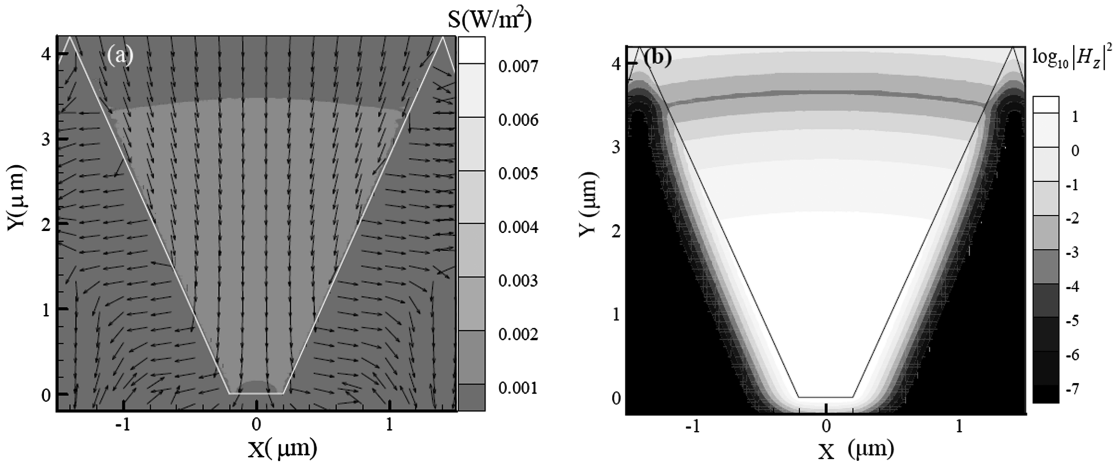

Fig. 9 Uncoated-grating case B-1 (without Al_2O_3) at $\theta = 0°$ and $\lambda = 11.4$ μm with reflectance of 0.652: a) Poynting vectors and b) square of the complex magnetic field strength in the logarithmic scale.

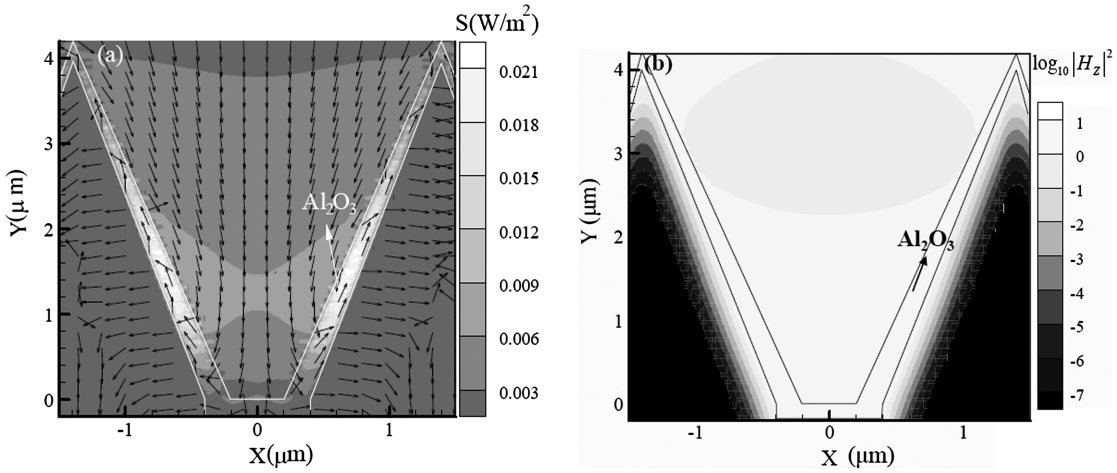

Fig. 10 Coated-grating case B-2 ($b = d = c = 0.2$ μm) at $\theta = 0°$ and $\lambda = 11.4$ μm with reflectance of 0.005: a) Poynting vectors and b) square of the complex magnetic field strength in the logarithmic scale.

IV. Conclusions

This study uses the finite difference time-domain method to examine the infrared radiative properties of microscale grating-surface structure of aluminum coated with alumina films. The main conclusions follow.

With the two different periodic geometries of aluminum coated with alumina films, some minima of the spectral reflectance will appear. Moreover, minimum spectral location shifts with wavelength when the alumina-film thickness changes. This study analyzes the reasons for the reflectance-minimum formation and variation with the alumina film.

First, it is due to the different geometries of the aluminum and alumina coating structures. Cavity resonances are formed in square-wave gratings, while surface waves are excited in sawtooth gratings. For the oxidized square-wave grating with a given film thickness, four different modes of cavity resonances are observed at different wavelengths. The resonance wavelengths will be changed as the oxide-film thickness increases. One mode of resonance is only formed in alumina films, while the others are excited in both alumina films and cavity. For the oxidized sawtooth grating, no cavity-resonance absorption peaks are observed; only one absorption peak exists, which is due to the surface waves absorbed by alumina films.

Second, it is due to alumina optical properties. The energy of the resonance is absorbed by alumina films when the resonance wavelength is within the range of 10.2 to 12 μm and absorbed by aluminum at the range of 2 to 10.2 μm, which is mainly due to the extinction coefficient of alumina. In conclusion, the results show that alumina film plays an important role in the propagation of electromagnetic waves and infrared radiative properties of the aluminum grating. The finding of this work may facilitate the design and applications of metallic gratings in cases in which the metal is easily oxidized.

Acknowledgments

The support of this work by the National Natural Science Foundation of China (50836002) and by the Program for Changjiang Scholars and Innovative Research Team in University (IRT0914) is gratefully acknowledged.

References

[1] Srituravanich, W., Fang, N., Sun, C., Luo, Q., and Zhang, X., "Plasmonic Nanolithography," *Nano Letters*, Vol. 4, No. 6, 2004, pp. 1085–1088. doi:10.1021/nl049573q

[2] Greffet, J.-J., Carminati, R., Joulain, K., Mulet, J.-P., Mainguy, S., and Chen, Y., "Coherent Spontaneous Emission of Light Due to Surface Waves," *Nature*, Vol. 416, 2002, pp. 61–64. doi:10.1038/416061a

[3] Sai, H., and Yugami, H., "Thermophotovoltaic Generation with Selective Radiators Based on Tungsten Surface Gratings," *Applied Physics Letters*, Vol. 85, No. 16, 2004, pp. 3399–3401. doi:10.1063/1.1807031

[4] Lee, B. J., Khuu, V. P., and Zhang, Z. M., "Partially Coherent Spectral Transmittance of Dielectric Thin Films with Rough Surfaces," *Journal of Thermophysics and Heat Transfer*, Vol. 19, No. 3, 2005, pp. 360–366. doi:10.2514/1.12512

[5] Boyden, S. B., and Zhang, Y., "Temperature and Wavelength-Dependent Spectral Absorptivities of Metallic Materials in the Infrared," *Journal of Thermophysics and Heat Transfer*, Vol. 20, No. 1, 2006, pp. 9–16. doi:10.2514/1.15518

[6] Shen, Y. J., Zhang, Z. M., Tsai, B. K., and Dewitt, D. P., "Bidirectional Reflectance Distribution Function of Rough Silicon Wafers," *International Journal of Thermophysics*, Vol. 22, No. 4, 2001, pp. 1311–1326. doi:10.1023/A:1010636914347

[7] Lee, H. J., and Zhang, Z. M., "Applicability of Phase Ray-Tracing Method for Light Scattering from Rough Surfaces," *Journal of Thermophysics and Heat Transfer*, Vol. 21, No. 2, 2007, pp. 330–336. doi:10.2514/1.26191

[8] Sentenac, A., and Greffet, J. J., "Design of Surface Microrelief with Selective Radiative Properties," *International Journal of Heat and Mass Transfer*, Vol. 37, No. 4, 1994, pp. 553–558. doi:10.1016/0017-9310(94)90127-9

[9] Queeney, K. T., Weldon, M. K., Chang, J. P., Chabal, Y. J., Gurevich, A. B., Sapjeta, J., and Opila, R. L., "Infrared Spectroscopic Analysis of the Si/SiO_2 Interface Structure of Thermally Oxidized Silicon," *Journal of Applied Physics*, Vol. 87, No. 3, 2000, pp. 1322–1330. doi:10.1063/1.372017

[10] Garcia-Vidal, F. J., and Martin-Moreno, L., "Transmission and Focusing of Light in One-Dimensional Periodically Nanostructured Metals," *Physical Review B*, Vol. 66, No. 15, 2002, pp. 155412. doi:10.1103/PhysRevB.66.155412

[11] Wang, A.-H., Hsu, P.-f., Chen, Y. B., and Liu, L.-H., "Modeling Infrared Radiative Properties of Heavily Doped Silicon Complex Gratings with Geometric Modifications," ASME 2009 2nd Micro/Nanoscale Heat & Mass Transfer International Conference, Shanghai, China, American Society of Mechanical Engineers, Paper 2009-18193, 2009.

[12] Wang, L. P., and Zhang, Z. M., "Resonance Transmission or Absorption in Deep Gratings Explained by Magnetic Polaritons," *Applied Physics Letters*, Vol. 95, No. 11, 2009, pp. 111904. doi:10.1063/1.3226661

[13] Lee, B. J., Wang, L. P., and Zhang, Z. M., "Coherent Thermal Emission by Excitation of Magnetic Polaritons Between Periodic Strips and a Metallic Film," *Optics Express*, Vol. 16, No. 15, 2008, pp. 11328–11336. doi:10.1364/OE.16.011328

[14] Palik, E. D., *Handbook of Optical Constants of Solids*, Academic Press, New York, 1985.

[15] Mathewson, A. G., and Myers, H. P., "Optical Absorption in Aluminium and the Effect of Temperature ," *Journal of Physics F: Metal Physics*, Vol. 2, No. 2, 1972, pp. 403–415. doi:10.1088/0305-4608/2/2/030

[16] Whitson, M. E., *Handbook of the Infrared Optical Properties of* Al_2O_3*, Carbon,* MgO*, and* ZrO_2, National Technical Information Service, Los Angeles, 1975.

[17] Kunz, K., and Luebbers, R., *Finite Difference Time Domain Method for Electromagnetics*, CRC Press, Boca Raton, FL, 1993.

[18] Berenger, J. P., "A Perfectly Matched Layer for the Absorption of Electromagnetic Wave," *Journal of Computational Physics*, Vol. 114, No. 2, 1994, pp. 185–200. doi:10.1006/jcph.1994.1159

[19] Teng, M., Wan, G., Zhen, Y., and Han, W., "A Review of Atmospheric Corrosion of Aluminum and Aluminum Alloys," *Corrosion Science and Protection Technology*, Vol. 16, No. 3, 2004, pp. 155–157 (in Chinese).

[20] Takakura, Y., "Optical Resonance in a Narrow Slit in a Thick Metallic Screen," *Physical Review Letters*, Vol. 86, No. 24, 2001, pp. 5601–5603. doi:10.1103/PhysRevLett.86.5601.

[21] Zhang, Z. M., *Nano/Microscale Heat Transfer*, McGraw–Hill, New York, 2007.

[22] Lakhtakia, A., and Polo, J. A., Jr., "Morphological Influence on Surface-Wave Propagation at the Planar Interface of a Metal Film and a Columnar Thin Film," http://arxiv.org/abs/0706.4300v1, 2007.